

Incomplete glycosylation during prion infection unmasks a prion protein epitope that facilitates prion detection and strain discrimination

Received for publication, January 24, 2020, and in revised form, May 31, 2020. Published, Papers in Press, June 8, 2020, DOI 10.1074/jbc.RA120.012796

Hae-Eun Kang^{1,‡}, Jifeng Bian^{1,‡}, Sarah J. Kane^{1,‡}, Sehun Kim¹, Vanessa Selwyn^{1,2}, Jenna Crowell¹, Jason C. Bartz³, and Glenn C. Telling^{1,2,*}

From the ¹Prion Research Center (PRC), Department of Microbiology, Immunology and Pathology, the ²Program in Cell and Molecular Biology, Colorado State University, Fort Collins, Colorado, and the ³Department of Medical Microbiology and Immunology, Creighton University, Omaha, Nebraska, USA

Edited by Paul E. Fraser

The causative factors underlying conformational conversion of cellular prion protein (PrP^C) into its infectious counterpart (PrP^{Sc}) during prion infection remain undetermined, in part because of a lack of monoclonal antibodies (mAbs) that can distinguish these conformational isoforms. Here we show that the anti-PrP mAb PRC7 recognizes an epitope that is shielded from detection when glycans are attached to Asn-196. We observed that whereas PrP^C is predisposed to full glycosylation and is therefore refractory to PRC7 detection, prion infection leads to diminished PrP^{Sc} glycosylation at Asn-196, resulting in an unshielded PRC7 epitope that is amenable to mAb recognition upon renaturation. Detection of PRC7-reactive PrP^{Sc} in experimental and natural infections with various mouse-adapted scrapie strains and with prions causing deer and elk chronic wasting disease and transmissible mink encephalopathy uncovered that incomplete PrP^{Sc} glycosylation is a consistent feature of prion pathogenesis. We also show that interrogating the conformational properties of the PRC7 epitope affords a direct means of distinguishing different prion strains. Because the specificity of our approach for prion detection and strain discrimination relies on the extent to which N-linked glycosylation shields or unshields PrP epitopes from antibody recognition, it dispenses with the requirement for additional standard manipulations to distinguish PrP^{Sc} from PrP^C, including evaluation of protease resistance. Our findings not only highlight an innovative and facile strategy for prion detection and strain differentiation, but are also consistent with a mechanism of prion replication in which structural instability of incompletely glycosylated PrP contributes to the conformational conversion of PrP^C to PrP^{Sc}.

Scrapie of sheep and chronic wasting disease (CWD) of deer, moose, elk, and other cervids, belong to a group of interrelated, fatal, transmissible neurodegenerative diseases caused by prions. Although natural or experimental prion transmission among members of the same species is a relatively efficient process, albeit following extended incubation periods, the infection

of humans with bovine spongiform encephalopathy and the resulting development of a variant of Creutzfeldt Jakob disease in young adults and teenagers (1) epitomizes the potential for prions to cross-species barriers. The continued emergence of novel animal prion diseases, including newly-discovered forms of CWD (2) in Scandinavian moose, reindeer, and European red deer, as well as a prion disease of camels in Northern Africa (3) not only highlights the unpredictable epidemiology of these disorders but also raises concerns over future additional zoonotic risks.

Prions are proteinaceous infectious particles devoid of either DNA or RNA (4). They are composed of PrP^{Sc}, the conformationally disrupted version of a benign host-encoded counterpart protein referred to as PrP^C. Agent replication occurs by a poorly understood process in which PrP^{Sc} imposes its infective conformation on PrP^C by means of interactive conformational templating, with transformation of additional PrP^C by the resulting PrP^{Sc}, which in turn leads to exponential prion accumulation (5). NMR spectroscopic analysis of bacterially expressed recombinant PrP (rPrP) provided an authentic, high-resolution structural model of PrP^C, which confirmed its predominantly α -helical status (6). Recently, a physically plausible atomic resolution model based on cryo-EM, X-ray fiber diffraction studies, and computational techniques proposed that PrP^{Sc} is structured as a four-rung β -solenoid (7). Although PrP^C and PrP^{Sc} share identical primary structures in a diseased host, their conformational differences are associated with distinctive biochemical properties. Thus, whereas PrP^C is monomeric and soluble in nondenaturing detergents, PrP^{Sc} is relatively resistant to protease digestion and forms insoluble aggregates in nondenaturing detergents. Although these physicochemical properties have provided useful operational hallmarks with which to distinguish PrP^{Sc} from PrP^C, the aggregating properties of PrP^{Sc} have presented significant impediments for high-resolution structural analysis. Considerable efforts have therefore been made to devise alternate means of discriminating between PrP^C and PrP^{Sc}, including attempts to isolate anti-PrP monoclonal antibodies (mAbs) capable of recognizing epitopes specific to each conformer. However, despite early promises, purportedly prion-specific mAbs (8, 9), ultimately failed to discriminate noninfectious from infectious PrP aggregates (10).

This article contains supporting information.

[‡]These authors contributed equally to this work.

* For correspondence: Glenn C. Telling, glenn.telling@colostate.edu.

Present address for Hae-Eun Kang: Foreign Animal Disease Division, Animal and Plant Quarantine Agency, Gimcheon-si, Gyeongsangbuk-do, Republic of Korea.

Like conventional infectious agents, prions exist as different strains with heritable properties that are subject to mutation under selective pressure (11, 12). Strain properties not only dictate the tempo and clinical/pathological outcomes of disease in their species of origin, but also influence the capacity of prions to transit species barriers (13). Although prion strain information is considered to be enciphered by distinct conformations of PrP^{Sc} (14, 15), our limited knowledge of PrP^{Sc} structure and inability to define strain-dependent conformational variability with any degree of precision has placed significant restrictions on our understanding of how prion proteins transmit heritable information in the absence of informational nucleic acids.

In addition to their structural and biochemical differences, PrP^C and PrP^{Sc} undergo diverse intracellular proteolytic processing events. PrP^C is subject to amino-terminal proteolytic cleavage at amino acids 110–111 within a segment of conserved hydrophobic amino acids to produce an ~17-kDa C-terminal fragment referred to as C1 (16, 17), whereas a longer C-terminal fragment, referred to as C2, with the same ~21-kDa apparent molecular mass as the protease-resistant core of PrP^{Sc}, accumulates in prion-infected brains (18, 19).

The primary structure of PrP contains two conserved glycan attachment sites at asparagine (Asn) residues 196 and 180 (mouse PrP numbering). *N*-Linked glycosylation involves enzymatic transfer of a lipid-linked oligosaccharide and covalent modification of the acceptor N of the consensus sequence N-X-T/S, where *X* is any amino acid except proline (Pro). Variable occupancy the two sites in PrP results in four possible glycosylated states: fully or hyperglycosylated PrP in which both glycan attachment sites are occupied; and three hypoglycosylated forms, including PrP, which is either monoglycosylated only at position 180 or 196, hereafter referred to as mono 1 and mono 2, respectively, and nonglycosylated PrP in which neither site is occupied. Not only full-length, but also the aforementioned amino-terminal processed forms of PrP are subject to differential glycosylation resulting in a complex distribution of upwards of 50 distinct PrP^C species (20).

Several groups including our own have isolated and characterized mAbs that react with specific subsets of these glycosylated PrP species (21–24). In this current study we asked whether reactivity of one such anti-PrP mAb, referred to as PRC7 (24), depended on the state of prion infection. We show that mAb PRC7 preferentially reacts with PrP^{Sc} produced during prion infection, and that this selective reactivity results from hypoglycosylation and consequent exposure of the PRC7 epitope in PrP^{Sc} relative to PrP^C. Our findings therefore embody a novel immunological strategy for prion detection and discrimination of PrP^{Sc} strain conformers using antibodies, the epitopes of which are exposed or shielded due to *N*-glycan occupancy of PrP.

Results

Characterizing the mechanism by which mAb PRC7 recognizes hypoglycosylated PrP

Our previous limited investigations of a novel conformation-dependent mAb referred to as PRC7 indicated that it recognized hypoglycosylated PrP; by contrast, the conformation-de-

pendent mAb PRC5 recognized the complete complement of full-length and proteolytically processed PrP glycoforms (24). Although the conformational dependence of these mAbs appeared incompatible with their abilities to recognize PrP on Western blots under conditions generally regarded as denaturing, we previously demonstrated that, subsequent to denaturing treatments, PrP refolds during Western blotting to a structure amenable to detection by these and other conformation-dependent antibodies (24). To more fully characterize the mechanism by which mAb PRC7 recognizes hypoglycosylated PrP, we expressed WT and mutated versions of mouse PrP (MoPrP) in rabbit kidney RK13 epithelial cells which express no endogenous PrP (Fig. 1, A and B). In Western immunoblots of extracts from RK13 cells expressing WT MoPrP, referred to as RK-M, mAb PRC5 reacted with variously glycosylated full-length and proteolytically processed derivatives of PrP^C with overlapping apparent molecular weights. Following PNGase F-mediated enzymatic removal of *N*-linked glycans, this array of PrP glycoforms resolved into deglycosylated ~27-kDa full-length PrP^C and ~17-kDa C1 (16, 17), as well as smaller amounts of the ~21-kDa C2 fragment (18, 19) (Fig. 1A). In contrast, whereas mAb PRC7 failed to recognize hyperglycosylated PrP and only detected low levels of ~27- and ~33-kDa PrP fragments in untreated RK-M cell extracts, PNGase F treatment resulted in increased levels of PRC7-reactive deglycosylated ~27-kDa full-length PrP and ~17-kDa C1 (Fig. 1B). Our results indicate the ~27-kDa PRC7-reactive species corresponds to full-length, nonglycosylated MoPrP, while the disappearance of the ~33-kDa PRC7-reactive fragment following PNGase F treatment demonstrates its partially glycosylated status. The differential reactivity of mAb PRC7 with PNGase F-treated and untreated RK-M cell extracts also confirms that PrP^C is a predisposed to full glycan occupancy.

To ascertain whether the partially glycosylated ~33-kDa PRC7-reactive species (Fig. 1B) resulted from *N*-glycan attachment at residue 180 or 196, we mutated each *N*-linked attachment signal sequence (Fig. 1G) and expressed the modified MoPrP constructs in RK13 cells. In cells expressing MoPrP where Asn-180 was changed to alanine (Ala), referred to as RK-N180A, reactivity with mAb PRC5 confirmed that inhibition of *N*-glycan attachment at this position prevented PrP hyperglycosylation; instead RK-N180A cells produced only mono 2 and nonglycosylated PrP (Fig. 1A). Because mAb PRC7 only reacted with nonglycosylated ~27-kDa full-length MoPrP under these conditions, we conclude that the partially glycosylated ~33-kDa PRC7-reactive species produced in RK-M cells is mono 1. Mutation of Asn-196 or Thr-198 to Ala also prevented PrP hyperglycosylation by inhibiting glycan attachment at this consensus sequence. In both cases, RK-N196A and RK-T198A cells produced nonglycosylated PrP and mono 1 PrP, increased levels of the latter being detectable by mAbs PRC5 and PRC7 (Fig. 1, C and D). Collectively these results show that PRC7 recognizes hypoglycosylated PrP comprised of ~27-kDa nonglycosylated and ~33-kDa mono 1 PrP but that it fails to react with PrP in which glycans are attached at Asn-196 including mono 2 and fully glycosylated PrP.

Our previous studies suggested that amino acid substitutions at tyrosine (Tyr) 154 or glutamine (Gln) 185 affected the

Targeting underglycosylated PrP^{Sc} as a basis for prion detection

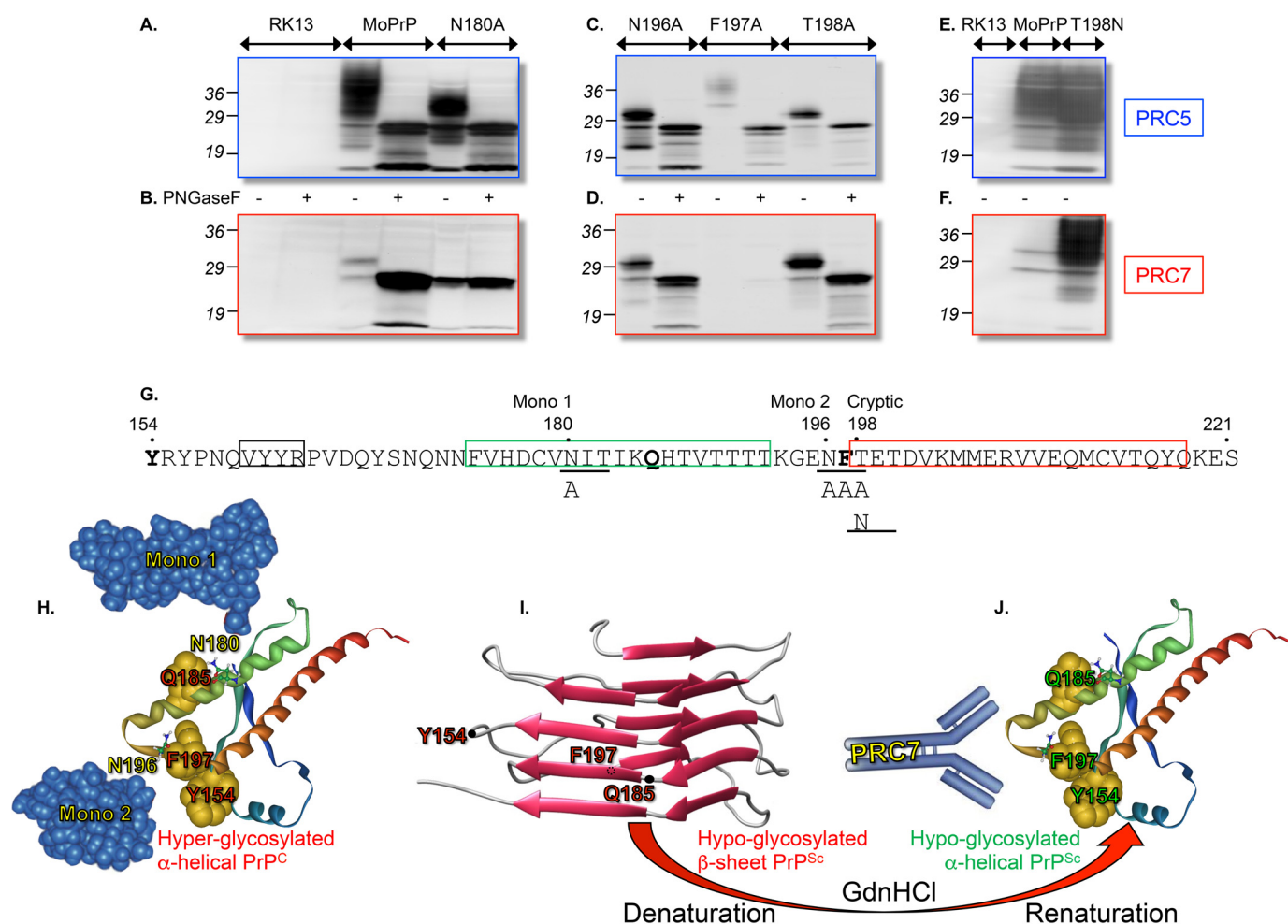


Figure 1. Characterization of the epitope of and mechanism by which mAb PRC7 recognizes hypoglycosylated PrP. A–F, immunoblots of PrP expressed in RK13 cells probed with mAbs PRC5 or PRC7. Cell extracts were either treated or not with PNGase F as indicated. RK13 refers to cells transfected with empty expression vector; in all other cases RK13 cells were engineered to express either WT or mutated MoPrP as indicated. Mutants are designated by the single amino acid code at a particular residue in the MoPrP sequence followed by the substituted amino acid. Positions of molecular mass marker proteins (kDa) are indicated. Equal amounts of total protein were loaded in all lanes of each immunoblot. G, MoPrP primary structure between residues 154 and 221. Locations of β -sheet region 2, α -helix 2, and α -helix 3 of PrP^C are indicated by black, green, and red boxed sequences, respectively. Residues affecting mAb PRC7 reactivity with MoPrP are in bold. Mono 1, mono 2, and the cryptic N-glycosylation consensus sequences are underlined. Residues mutated in expressed constructs are shown below the WT sequence. H–J, locations of PRC7 epitope components and N-glycan attachment sites in proposed three-dimensional structures of PrP^C (H and J) and PrP^{Sc} (I). In H, locations of N-glycan attachment are in yellow. The figure in I showing the locations of PRC7 epitope components in the proposed PrP^{Sc} structure is adapted from (7). In J, denaturation and refolding of PrP^{Sc} leads to reconstitution of the functional PRC7 epitope in α -helical PrP. In H and I, PRC7 epitope components either shielded from recognition by mono 2 or in the incorrect conformation in nonglycosylated PrP^{Sc} are indicated in red, whereas in J, unshielded epitope components refolded into the appropriate conformation for PRC7 recognition after denaturation of PrP^{Sc} are shown in green.

capacity of PRC7 to recognize MoPrP (24) (Fig. 1G). During mutagenesis of the mono 2 attachment site, we found that recognition of PrP by PRC7 was also compromised when phenylalanine (Phe) at residue 197 was mutated to Ala (Fig. 1D). Because the N-glycosylation consensus sequence accommodates any amino acid except Pro at this position, these findings suggest that Phe-197 is a component of the PRC7 epitope. In support of this proposal, PRC7 reactivity was also compromised when RK-F197A cell extracts were treated with PNGase F (Fig. 1, C and D).

Molecular modeling studies in which we mapped residues Tyr-154, Gln-185, and Phe-197 within the tertiary structure of PrP^C, deduced by NMR spectroscopic analysis of rPrP (6), revealed their alignment within a solvent-exposed interface coincident with the location of N-glycan attachment at Asn-

196 (Fig. 1H). Our findings therefore collectively indicate that these amino acid residues, which are discontinuous within the primary structure of PrP, contribute to PRC7 epitope recognition in the structural context of PrP^C, but that the epitope is shielded from detection when glycans are attached to residue Asn-196 (Fig. 1H).

Additional mutagenesis studies are consistent with this interpretation. Although cells expressing a mutation of Thr at residue 198 to Asn, referred to as RK-T198N, expressed PrP in which mono 2 attachment was abolished at Asn-196, this substitution coincidentally formed a cryptic N-glycan attachment site at Asn-198 (Fig. 1G). RK-T198N cells produced fully glycosylated PrP, which was amenable to detection not only by PRC5, but also by PRC7 (Fig. 1, E and F). We conclude that this two amino acid shift in N-glycan attachment to residue 198,

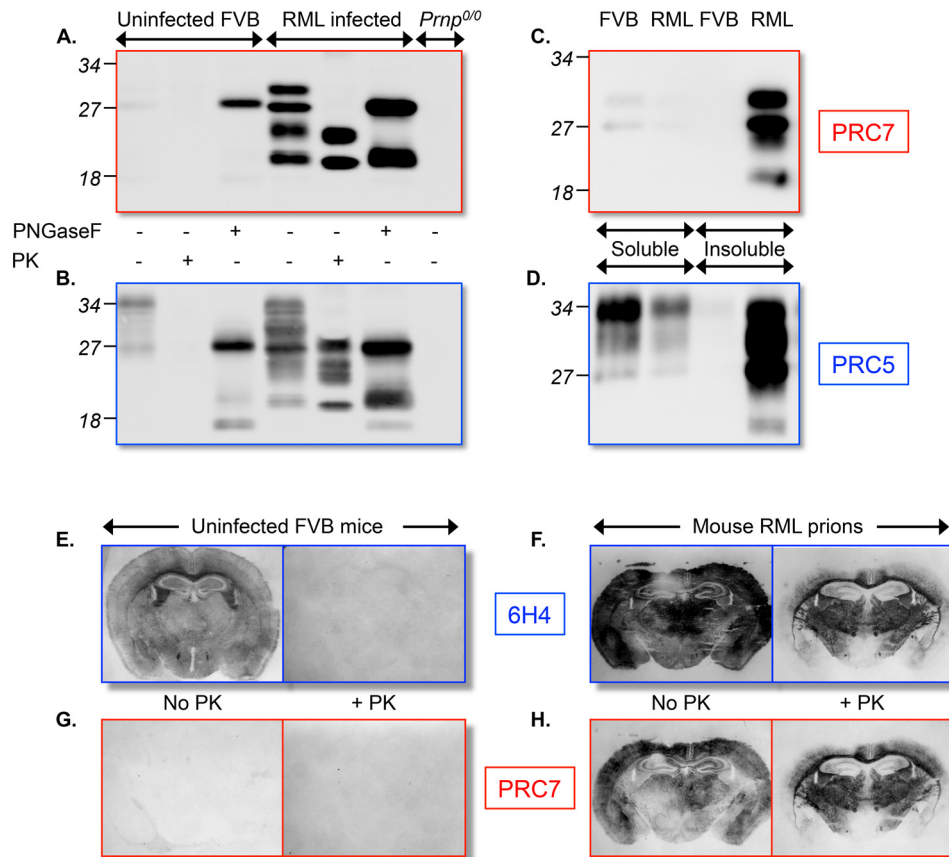


Figure 2. PRC7 detects hypoglycosylated PrP^{Sc}. A and B, immunoblots of PrP in brain extracts from RML infected and age-matched uninfected FVB mice probed with mAbs PRC5 or PRC7. *Prnp*^{0/0} mice that express no PrP as a result of disruption of the gene coding sequence. Extracts were treated or not with PNGase F or PK as indicated. The positions of molecular mass marker proteins (kDa) are indicated. 20 µg of total protein were loaded per lane. C and D, immunoblots of detergent-soluble and -insoluble PrP following ultracentrifugation of 50 µg of total protein from uninfected and RML-infected FVB brain extracts probed with mAbs PRC5 or PRC7. E–H, PrP distribution in PK-treated or -untreated histoblotted coronal sections of RML infected FVB, and age-matched uninfected mice probed with either 6H4 or PRC7.

which is the first amino acid of α -helix 3, relieves the steric constraints that prevent access of mAb PRC7 to its epitope in PrP^C, which normally occurs when glycans are linked to residue Asn-196 in the loop region connecting α -helices 2 and 3.

Preferential detection of hypoglycosylated PrP during prion infection by immunoblotting with PRC7

In light of our findings that suboptimal PRC7 reactivity in uninfected cells reflects a propensity for MoPrP^C to be full glycosylated, we next investigated whether the ability of PRC7 to detect hypoglycosylated PrP depended on the state of prion infection. To initially address this, we compared PRC7 reactivity in brain extracts of RML prion-infected mice with those of uninfected, age-matched counterparts. Although PRC7-reactive PrP was barely measurable in brain extracts of uninfected mice, PNGase F treatment facilitated detection of deglycosylated, PRC7-reactive full-length PrP (Fig. 2A); in contrast, mAb PRC5 detected hyperglycosylated, protease-sensitive full-length PrP^C and C1 in uninfected mouse brain extracts, which resolved into ~27- and 17-kDa deglycosylated equivalents after PNGase F treatment, as well as a minor fragment migrating at ~22-kDa (Fig. 2B). In sharp contrast to the low levels of PRC7-reactive hypoglycosylated PrP in uninfected FVB mouse brains, in RML-infected brain extracts mAb PRC7 detected

abundant amounts of ~27-kDa nonglycosylated and ~33-kDa monoglycosylated full-length PrP, as well as ~21-kDa nonglycosylated and ~25-kDa monoglycosylated C2, which persisted after proteinase K (PK) treatment (Fig. 2A). Accumulation of endoproteolytically-cleaved C2 is a characteristic of RML prion infection (19). The presence of fragments of equivalent apparent molecular weights within an array of glycosylated and nonglycosylated PrP fragments was confirmed by immunoblotting of infected brain extracts with PRC5 (Fig. 2B). We conclude that the selective reactivity of PRC7 with hypoglycosylated PrP produced under conditions of infection provides a specific immunologic means to confirm that aberrant PrP glycosylation is a feature of RML prion infection in mice.

The foregoing results indicated that the properties of PRC7-reactive hypoglycosylated PrP produced during infection were coincident with those of PrP^{Sc} constituting RML prions. To substantiate this proposition, we isolated detergent-soluble and -insoluble forms of PrP following high-speed centrifugation in the presence of Sarkosyl. As expected, PRC5-reactive PrP^C partitioned in the detergent-soluble fractions of uninfected and, consistent with previous findings (25), to a lesser extent in RML-infected mouse brain extracts (Fig. 2C). Whereas reactivity with PRC5 demonstrated that both detergent-soluble PrP^C and -insoluble PrP^{Sc} contained hyperglycosylated PrP, PRC7-

Targeting underglycosylated PrP^{Sc} as a basis for prion detection

reactive hypoglycosylated PrP partitioned predominantly in the detergent-insoluble fraction of RML-infected brain extracts comprising PrP^{Sc} (Fig. 2C). Relatively minor amounts of hypoglycosylated PrP were present in detergent-soluble preparations of uninfected, and to an even lesser extent in detergent-soluble preparations of infected mouse brains (Fig. 2C). Our results confirm that although only a minor fraction of detergent-soluble PrP^C is incompletely glycosylated, hypoglycosylated PrP is a significant constituent of detergent-insoluble PrP^{Sc} aggregates resulting from RML prion infection.

The selective production of hypoglycosylated PrP during RML prion infection, suggested the possibility of using mAb PRC7 to characterize the distribution of PrP^{Sc} in the brains of infected mice. To address this, we assessed the patterns of PRC7-reactive hypoglycosylated PrP present in histoblotted brain sections (63) of terminally diseased RML-infected compared with age-matched uninfected controls. Because they fail to discriminate between PrP^C and PrP^{Sc}, mAbs such as 6H4 (8) rely on the relative protease sensitivity of PrP^C for PrP^{Sc} detection by immunoblotting (Fig. 2, E and F); accordingly, mAb 6H4 detected PrP in nonPK-treated histoblotted sections from uninfected as well as infected mouse brains (Fig. 2, E and F). In contrast, mAb PRC7 failed to react with PrP in brain sections of uninfected mice and reacted with hypoglycosylated PrP only in histoblotted brain sections of mice infected with mouse-adapted RML scrapie prions (Fig. 2, G and H). These findings lend additional support to the notion that mAb PRC7 detects hypoglycosylated PrP^{Sc} only under conditions of prion infection, and that PRC7 provides a means of distinguishing PrP^{Sc} from PrP^C without reliance on their differential resistance to protease treatment.

ELISA detection of hypoglycosylated PrP^{Sc}

The preferential reactivity of mAb PRC7 with hypoglycosylated PrP^{Sc} motivated us to create ELISA platforms to monitor prion infection. First, we used indirect ELISAs to confirm the reactivities of PRC7 and PRC5 with mouse and elk rPrP (Fig. 3A), the folded structures of which are equivalent to that of their PrP^C counterparts (6) and, as a result of prokaryotic expression, are nonglycosylated. Next, to ultimately facilitate detection of hypoglycosylated PrP^{Sc} in tissue extracts, we also used mouse and elk rPrP to establish a sandwich ELISA format. We found that the most effective means of mouse or elk rPrP detection resulted from a combination in which PRC7 immobilized to ELISA plates acted as capture mAb and, because their epitopes are nonoverlapping (24), mAb PRC5 acted as the detection antibody (Fig. 3A).

We next investigated the capacity of this sandwich ELISA, referred to as the 7-5 ELISA, to discriminate RML prion-infected brain extracts from those of uninfected mice. We performed 7-5 ELISA across a range of protein amounts extracted from brains of RML prion-infected mice, age matched uninfected FVB counterparts. FVB/*Prnp*^{0/0} mice, which express no PrP served as a negative control. Because we previously reported that subsequent to denaturation PrP^C and PrP^{Sc} both renature to a correctly folded structure amenable to detection by conformation-dependent antibodies including PRC5 and

PRC7 (24), we also assessed the effects of GdnHCl pretreatment of brain extracts on the capacity of the 7-5 ELISA to detect hypoglycosylated PrP. Without GdnHCl denaturation the 7-5 ELISA failed to detect hypoglycosylated PrP in either RML-infected or uninfected FVB brain extracts (Fig. 3B). By contrast, GdnHCl pretreatment of the same brain extracts showed that PRC7-reactive hypoglycosylated PrP was present exclusively in the brains of RML-infected mice (Fig. 3C). The responses of FVB and FVB/*Prnp*^{0/0} brain extracts in the 7-5 ELISA were uniformly negative, regardless of whether or not samples were subjected to GdnHCl treatment (Fig. 3, B and C). We conclude that the inability of the 7-5 ELISA to detect hypoglycosylated PrP in uninfected FVB brains reflects the hyperglycosylated status of PrP^C, and that uninfected brains contain undetectable levels of hypoglycosylated PrP by 7-5 ELISA (Fig. 3C). By contrast, because the 7-5 ELISA only detects hypoglycosylated PrP during prion infection, our results provide further evidence that PrP^{Sc} produced during RML prion infection is comprised of hypoglycosylated PrP.

Our findings also indicate that the specificity of the 7-5 ELISA for PrP^{Sc} derives from two features of the PRC7 epitope. Specifically, full glycan occupancy at Asn-196 in hyperglycosylated PrP^C prevents access of PRC7 to its underlying epitope. In contrast, whereas hypoglycosylation of PrP^{Sc} means that the PRC7 epitope is not shielded from detection by glycan attachment at Asn-196, epitope recognition requires reorientation of its constituent amino acids from an inactive conformation in PrP^{Sc} to its functional state in the context of globular, α -helical PrP (Fig. 1J). Support for this mechanism derives from the four-rung β -solenoid model of PrP^{Sc} in which the proposed constituent residues of the PRC7 epitope are separated in three-dimensional space (7) (Fig. 1I) compared with the alignment of these discontinuous residues in the structural context of PrP^C (Fig. 1H).

To further validate the specificity of the 7-5 ELISA for PrP^{Sc} detection, we replaced the PRC7 capture mAb with the D13 antibody, which recognizes the PrP^C conformation and does not distinguish PrP glycoforms (26). In contrast to the 7-5 ELISA, this 13-5 sandwich ELISA detected PrP in both infected and uninfected brain extracts; moreover, D13 reactivity was not dependent upon GdnHCl pretreatment (Fig. 3, D and E). In the absence of GdnHCl pretreatment, the 13-5 ELISA detected PrP in brains of RML-infected mice at levels that were lower ($p \leq 0.0001$) than those found in uninfected age-matched controls (Fig. 3D), whereas GdnHCl pretreatment of brain extracts resulted in increased detection of PrP in RML-infected compared with uninfected brain extracts (Fig. 3E). We interpret this to mean that under nondenaturing conditions D13 detects natively conformed PrP^C, in part because this finding is also in accordance with previous findings (26). Consistent with this interpretation and with additional previous findings (25), the lower levels of D13-reactive, nondenatured PrP produced during prion infection reflect a reduced pool of available PrP^C. In contrast, the increased levels of detectable PrP following denaturation reflect the combined contributions of PrP^C as well as renatured PrP^{Sc} (27).

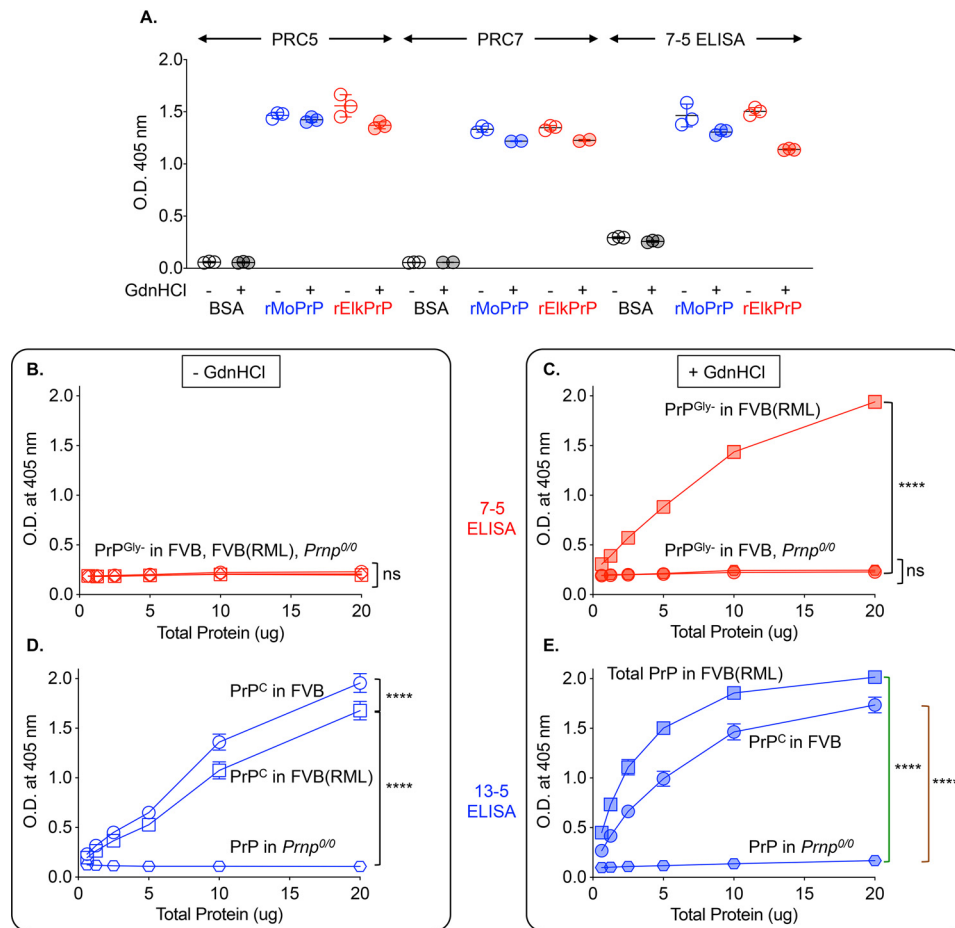


Figure 3. ELISA detection of PRC7-reactive hypoglycosylated PrP^{Sc}. A, PRC5 and PRC7 react with nonglycosylated bacterially expressed elk and mouse rPrP in indirect ELISA formats, and in the 7-5 sandwich ELISA where PRC7 and PRC5 are capture and detection antibodies, respectively. Samples were treated or not with GdnHCl as indicated. B and C, capture mAb PRC7 (red symbols) distinguishes between uninfected and RML prion-infected brain homogenates in the absence of PK digestion by virtue of its selective reactivity with hypo-glycosylated PrP^{Sc}. Reactivity with PRC7-reactive PrP^{Sc} requires denaturation/renaturation from PrP^{Sc} to the PrP^C conformation. D and E, capture Ab D13 (blue symbols) fails to distinguish between uninfected and RML prion-infected brain homogenates. In B–E, detection mAb is PRC5. In B–E, ELISAs were performed on brain extracts containing different amounts of total protein. RML-infected FVB mouse brain homogenates (squares); age-matched uninfected FVB mouse brain homogenates (circles); brain extracts from Pmp^{0/0} mice (hexagons). No denaturant, open symbols (B and D); treatment with GdnHCl, shaded symbols (C and E). Error bars refer to mean \pm S.D. of analyzed values from three to seven brains in each group. ns, $p > 0.05$; ****, $p \leq 0.0001$. Pairwise analysis by Student's *t* test calculated at 20 μ g of total protein.

Evolution of hypoglycosylated PrP^{Sc} correlates with increasing prion titers during RML infection

To further correlate PRC7-reactive hypoglycosylated PrP^{Sc} with conventional measures of prion pathogenesis and to address its evolution during prion infection we performed longitudinal analysis of brain extracts from FVB mice harvested at regular intervals after intracerebral inoculation with RML prions. Inoculated mice that were allowed to progress to the clinical phase ($n = 14$) developed signs of neurological disease with a mean time to onset of 118 ± 2 days (mean \pm S.E.) (Fig. 4A). Hypoglycosylated PrP^{Sc} was detected by 7-5 ELISA ~60 days prior to the onset of clinical signs, and levels continued to rise for the succeeding 80 days (Fig. 4, A and C). The time of first detection and subsequent accumulation of hypoglycosylated PrP^{Sc} detected by 7-5 ELISA coincided with that of protease-resistant PrP^{Sc} detected by immunoblotting (Fig. 4, C and D). Analysis of infectious prion titers using a modified scrapie cell assay (28–30) (Fig. 4B) showed that, whereas prion loads persisted at $\sim 10^{5.0}$ infectious units/g of brain during the initial

30 days after prion challenge, thereafter infectivity exponentially increased to reach maximal levels of $10^{8.67}$ infectious units/g during the clinical phase. These analyses show that hypoglycosylated and protease-resistant PrP^{Sc} share equivalent kinetics of formation, which coincide with increasing RML prion titers, and that the lower limit of PRC7-reactive hypoglycosylated PrP^{Sc} detection corresponds to a titer of $\sim 10^{7.32}$ infectious units/g attained at the midpoint of the exponential phase of RML prion replication.

Hypo-glycosylation of PrP^{Sc} is a consistent feature of prion replication

Having established the specificity of the 7-5 ELISA for detecting hypoglycosylated PrP^{Sc} during RML prion infection, we next investigated its capacity to detect PrP^{Sc} in brain extracts of diseased mice infected with additional scrapie strains that were experimentally adapted in WT mice. The 7-5 ELISA detected hypoglycosylated PrP^{Sc} exclusively in the brains of mice infected with mouse-adapted scrapie 22L and

Targeting underglycosylated PrP^{Sc} as a basis for prion detection

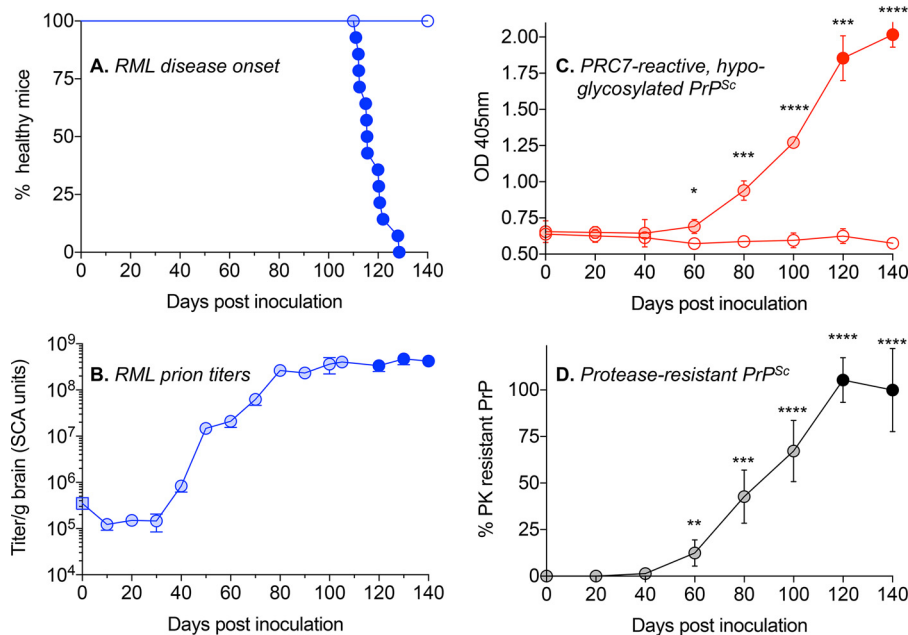


Figure 4. Evolution of PRC7-reactive hypoglycosylated and protease-resistant PrP^{Sc}, and correlation with prion titers during RML prion infection in mice. Animals were collected at the indicated times following challenge with RML prions. *A*, survival of RML-infected FVB mice. *B*, RML prion titers determined by scrapie cell assay using RK-M cells. *Error bars*, S.E. from analysis of five to six mice. *C*, levels of hypoglycosylated PrP^{Sc} in 20 µg of brain extracts determined by 7-5 ELISA. *D*, levels of protease-resistant PrP^{Sc} in infected mice normalized to levels detected in the brains of diseased mice in the clinical phase. In *A–D*, shaded symbols, preclinical phase; filled symbols, clinically affected mice; open symbols, mock infected. In *C* and *D*, error bars, S.D. from analysis of five to six mice.

139A strains, but not in the brains of their uninfected C57Bl/6 counterparts (Fig. 5*A*). Further confirming that the properties of hypoglycosylated PrP^{Sc} overlapped with those of protease-resistant PrP^{Sc}, treatment of infected brain extracts with PK had no effect on the capacity of the 7-5 ELISA to detect hypoglycosylated PrP^{Sc} in the brains of mice infected with 22L or 139A prions (Fig. 5*A*). These findings indicate that accumulation of hypoglycosylated PrP^{Sc} is a general consequence of infection with diverse mouse-adapted scrapie prions.

We next asked whether aberrant PrP glycosylation featured in the replication of naturally occurring prions from other species where the primary structure of PrP is known to contain the predicted PRC7 epitope (24). Western blotting experiments confirmed that PRC7 recognized hypoglycosylated PrP^{Sc} in the brains of mink infected with transmissible mink encephalopathy (TME) prions (Fig. S1*A*), and in the brains of CWD-infected gene-targeted mice expressing elk PrP referred to as GtE226^{+/+} (31) (Fig. S1*A*). In accordance with our findings with experimentally adapted mouse prion strains, hypoglycosylated PrP^{Sc} was also detected by 7-5 ELISA in the brains of TME infected mink (Fig. 5*B*), and in CWD-infected GtE226^{+/+} and GtQ226^{+/+} (31) (Fig. 5, *C* and *D*), but not in age-matched uninfected counterparts (Fig. 5, *B–D*). Our findings demonstrate that the accumulation of hypoglycosylated PrP^{Sc} is a consistent feature of prion replication.

CWD diagnosis in naturally affected deer and elk by 7-5 ELISA

Our ability to detect hypoglycosylated deer or elk PrP^{Sc} following experimentally controlled CWD infection of Gt mice encouraged us to investigate the diagnostic potential of the 7-5 ELISA in animals naturally affected with CWD prions. To

address this, we analyzed brain extracts of 19 CWD-affected deer and elk by 7-5 ELISA (Fig. 5*E*). Disease status was independently verified by transmission of CWD prions to susceptible transgenic (Tg) mice (32) (Fig. 5*E*), and/or by detection of protease-resistant PrP^{Sc} by immunoblotting (Fig. 5*F*). Using the 7-5 ELISA, levels of detectable hypoglycosylated PrP^{Sc} in all CWD samples exceeded a baseline of 5 S.D. above a mean OD value derived from 7-5 ELISA analysis of brain extracts from 20 uninfected deer and elk (Fig. 5*E*). There was positive correlation between levels of PRC7-reactive hypoglycosylated PrP^{Sc}, protease-resistant PrP^{Sc}, and CWD prion incubation times (Fig. 5, *E* and *F*).

Progressive refolding of the nonglycosylated, conformationally silent PRC7 epitope as a means of probing strain-related structural differences in PrP^{Sc}

Although multiple lines of evidence contend that prion strain information is enciphered within the conformation of PrP^{Sc} (14, 15), established methods to discern strain-dependent conformational differences rely on indirect measurements of residual PrP^{Sc} protease resistance after treatments with increasing concentrations of denaturant, followed by immunodetection with nondiscriminatory antibodies (33). The concordant properties of hypoglycosylated and protease-resistant PrP^{Sc}, and our finding that the nonglycosylated PRC7 epitope in PrP^{Sc} requires renaturation to a detectable conformation (Fig. 1, *I* and *J*) suggested a more direct approach to probe prion strain conformational differences. To accomplish this, we measured progressive accessibility of the nonglycosylated PRC7 epitope in PrP^{Sc} after denaturation and refolding over a range of GdnHCl concentrations, referred to as 7-5 conformational

Targeting underglycosylated PrP^{Sc} as a basis for prion detection

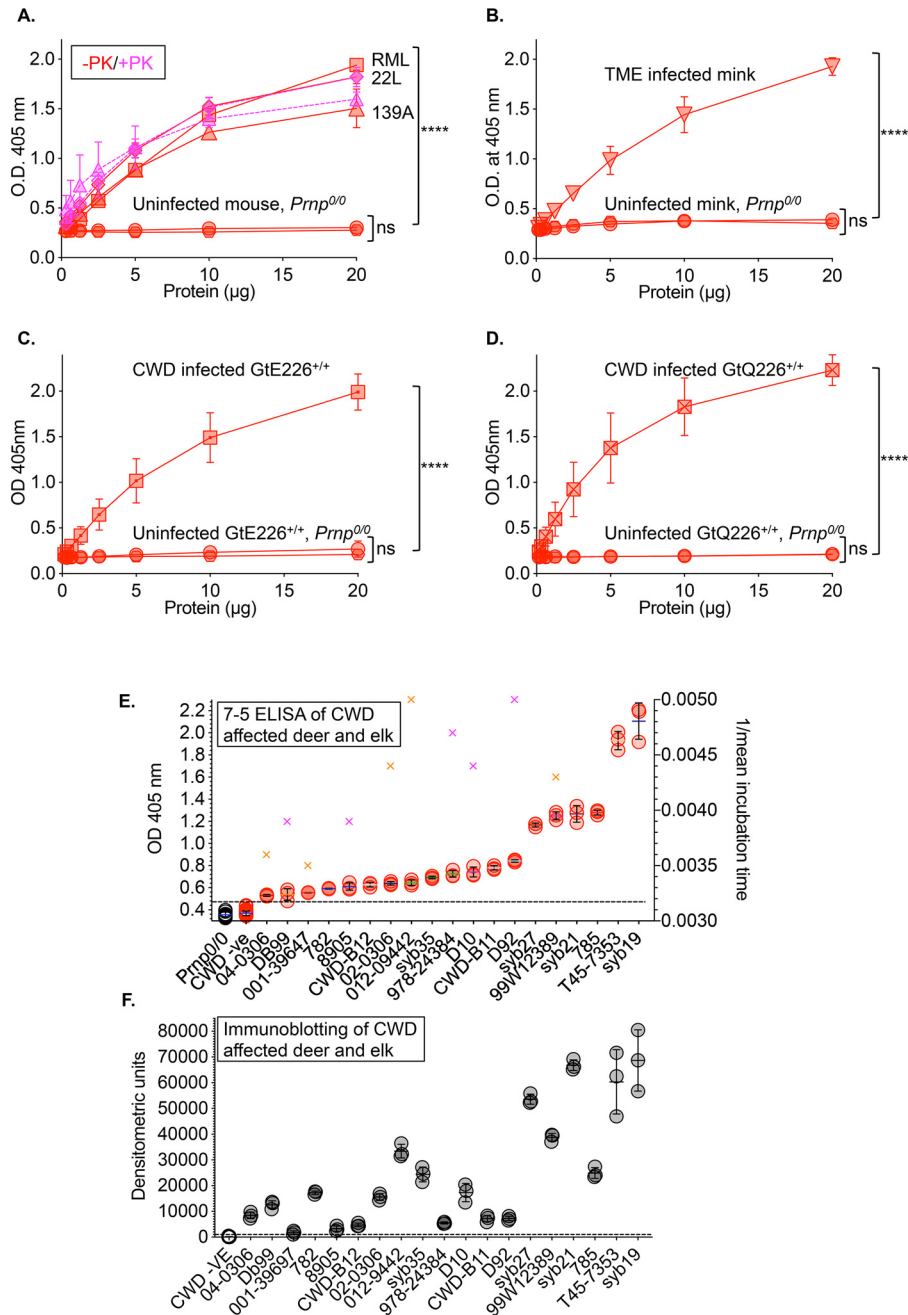


Figure 5. Accumulation of hypoglycosylated PrP^{Sc} is a universal feature of prion disease. PRC7 detects hypoglycosylated PrP^{Sc} in the 7-5 ELISA as a result of infection of: *A*, mice with multiple experimentally adapted mouse prion strains; *B*, mink infected with TME prions; *C* and *D*, gene targeted mice expressing cervid PrP with Glu or Gln at residue 226. In *A–D*, ELISAs were performed on brain extracts containing different amounts of total protein. In *A*, RML-infected FVB mice (squares); 22L-infected C57Bl/6 mice (diamonds); 139A-infected C57Bl/6 mice (triangles). Dotted lines and purple symbols for 22L and 139A, PK-treated samples. Mean ± S.D. in *A–D* were derived from triplicate experimental replicates of at least three and up to nine animals per group. *ns*, $p > 0.05$; ****, $p \leq 0.0001$. Pairwise analysis by Student's *t* test calculated at 20 μg of total protein. Diagnostic sensitivity and specificity of 7-5 ELISA for measuring PrP^{Sc} (*E*) and immunoblotting of protease resistant PrP^{Sc} (*F*) in brain extracts from CWD affected deer and elk. Shaded bars, diseased deer or elk; unshaded, disease-free deer or elk ($n = 20$); black bar, *Pmp^{0/0}*. Black dashed line, five mean ± S.D. above O.D. value of uninfected deer and elk. Right y axis in *E*, reciprocal of mean incubation times of deer CWD (magenta crosses) or elk CWD (orange crosses) in TgD. In *E* and *F*, error bars represent mean ± S.D. of triplicate experimental replicates of each sample.

stability analysis (7-5 CSA). We anticipated that a gradual rise in 7-5 ELISA signal in response to increasing GdnHCl concentrations would be a measure of the proportion of hypoglycosylated PrP^{Sc} in which the PRC7 epitope is refolded into a conformation amenable to capture by immobilized mAb PRC7, and that differences in the relative ease or difficulty of epitope renaturation would be reflective of conformational differences

between hypoglycosylated PrP^{Sc} constituting various prion strains.

We performed 7-5 CSA on brain extracts from WT mice infected with various mouse-adapted scrapie prions, as well as GtE226^{+/+} and GtQ226^{+/+} mice infected with deer and elk CWD prions (Fig. 6). Confirming that mouse, deer, and elk PrP^C are invariably hyperglycosylated, PRC7-reactive PrP was

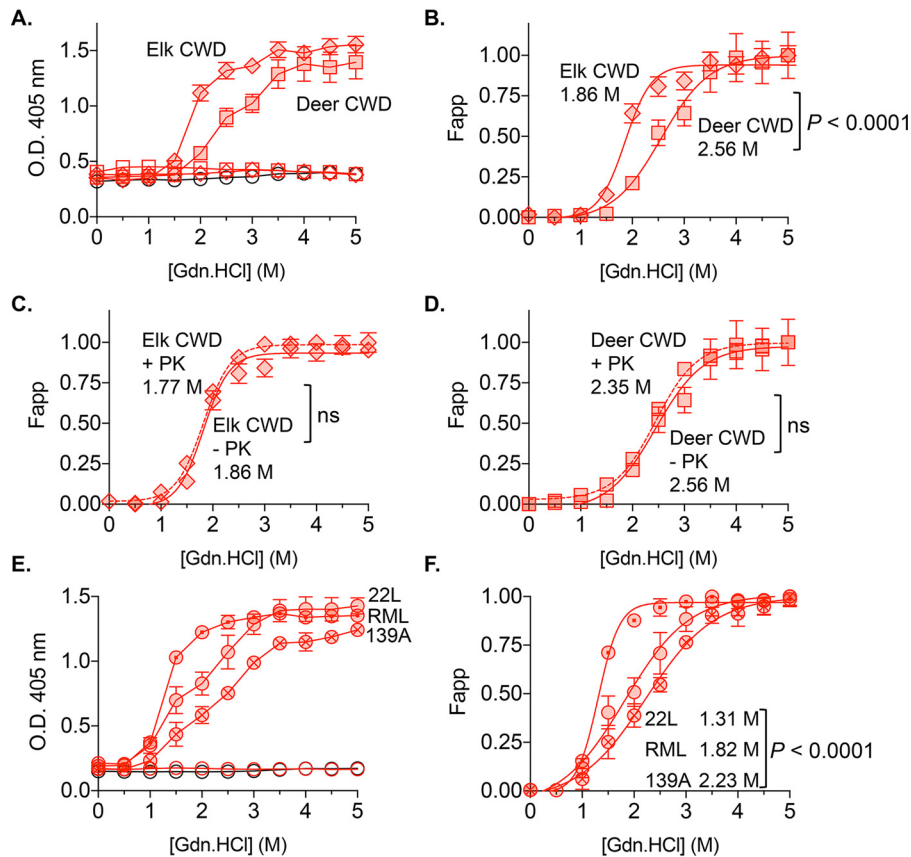


Figure 6. Denaturant-dependent reconfiguration of the hypoglycosylated PRC7 epitope in PrP^{Sc} as a means of probing conformational differences between prion strains. A–D, open red squares, uninfected GtQ226^{+/+} mice ($n = 9$ mice); shaded red squares, GtQ226^{+/+} mice infected with deer CWD prions ($n = 12$ mice); open red diamonds, uninfected GtE226^{+/+} mice ($n = 9$ mice); shaded red diamonds, GtE226^{+/+} mice infected with elk CWD prions ($n = 15$ mice); open black circles, Prnp^{0/0} mice ($n = 9$ mice). C and D, dashed lines, treatment of infected GtQ226^{+/+} ($n = 12$) and GtE226^{+/+} ($n = 15$) mouse brain homogenates with PK. E and F, shaded red circles, C57BL/6 mice infected with RML ($n = 9$ mice); shaded red dotted circles, C57BL/6 mice infected with 22L ($n = 9$ mice); shaded red crossed circles, C57BL/6 mice infected with 139A ($n = 9$ mice); open red circles, uninfected C57BL/6 mice ($n = 9$ mice); open black circles, Prnp^{0/0} mice ($n = 9$ mice). A and E, raw 7-5 ELISA readings. B–D and F, normalized, best fit data. Error bars indicate mean \pm S.D. Significance relates to differences between 7-5 CSA_{1/2} values from best-fitted curves.

undetectable in the brains of uninfected mice over the full range of GdnHCl concentrations (Fig. 6, A, E, and G). In contrast, we observed concentration-dependent detection of the denatured and refolded hypoglycosylated PrP^{Sc} PRC7 epitope in the brains of infected mice following GdnHCl treatment (Fig. 6, A–H).

Denaturation/refolding of hypoglycosylated PrP^{Sc} in the brains of CWD-infected GtE226^{+/+} and GtQ226^{+/+} mice produced distinct 7-5 CSA renaturation profiles that were indicative of differing conformations of elk and deer CWD prions (Fig. 6A). Although in both cases the PRC7 epitope in PrP^{Sc} remained inaccessible to detection up to ~ 1.0 M GdnHCl, progressive epitope refolding resulted in maximal detection at ~ 3.5 M for elk PrP^{Sc}, and ~ 4.0 M for deer PrP^{Sc}. We calculated the concentration of GdnHCl required to produce half-maximal renaturation of the PRC7 epitope to facilitate capture and detection (7-5 CSA_{1/2}) as a measure of relative conformational stability of hypoglycosylated PrP^{Sc}. The different mean 7-5 CSA_{1/2} values of elk and deer PrP^{Sc} of 1.86 and 2.56 M, respectively ($p \leq 0.0001$), supported the divergent conformational properties of deer and elk CWD prions (Fig. 6B). In accordance with our finding that PK had no effect on the capacity of the 7-5 ELISA to detect 22L or 139A prions (Fig. 5A), PK treatment of

CWD-infected GtE226^{+/+} and GtQ226^{+/+} brain extracts had no effect on the outcomes of the 7-5 CSA, or on the resulting 7-5 CSA_{1/2} values of deer or elk PrP^{Sc} (Fig. 6, C and D). Because these results agree with our previous findings of conformational differences between elk and deer PrP^{Sc} (12, 31, 32), we conclude that the 7-5 CSA represents a feasible approach to discern prion strain differences based on the conformational properties of the PRC7 epitope.

Renaturation curves of hypoglycosylated PrP^{Sc} produced in response to infection with 22L, 139A, and RML prions showed reproducibly distinct 7-5 CSA_{1/2} values of 1.31, 1.82, and 2.23 M, respectively ($p \leq 0.0001$) (Fig. 6, E and F). Collectively our findings implicate the tertiary structural region defined by the PRC7 epitope in strain-dependent structural variation of PrP^{Sc} and demonstrate that the 7-5 CSA is a sensitive and specific strategy to detect conformational differences between prion strains.

Discussion

Defining the structural features, which distinguish PrP^C and PrP^{Sc} is central to the prion hypothesis, yet the detailed mechanism underlying this conformational conversion remains

obscure. Using a novel immunological framework to discriminate between infectious and normal PrP, we show that whereas PrP^C is predisposed to complete occupancy of *N*-glycan attachment sites, this is not the case for PrP^{Sc}, which by comparison, is consistently under-glycosylated. *N*-Glycosylation is implicated in protein folding and stability as well as oligomerization and aggregation (34, 35), which are the cardinal features distinguishing PrP^C from PrP^{Sc}. Our findings are therefore consistent with a mechanism of prion replication in which the relative instability of hypoglycosylated PrP is a precipitant factor in the conformational conversion of PrP^C to PrP^{Sc}.

The role of *N*-glycosylation in the biology of PrP and prion formation has been the subject of investigation and debate (36), until now without providing clear answers. For example, previous studies have revealed conflicting effects of PrP glycosylation status on transmissibility and *in vitro* prion amplification (37–43). Whereas mutational analysis of the two conserved *N*-glycosylation sequences of PrP has been repeatedly employed in cell-based and transgenic mouse models of prion replication (44–48), this approach is not without drawbacks. Reports of altered prion transmissibility in genetically altered mouse models have relied on Thr to Ala or Asn to Thr substitutions at the PrP glycosylation sites (45–48). Because these substitutions also affect processing of PrP through the secretory pathway (49, 50), and changes in PrP^C primary structure elicit unpredictable effects on prion propagation ranging from the complete inhibition of PrP^C to PrP^{Sc} conversion (51) to alteration in the abilities of PrP^C to select distinct prion strain conformations (31, 32, 52–54), it has been difficult to precisely discern the overlapping effects of these PrP glycan-deficient mutations on prion pathogenesis.

The approach taken here bypasses the drawbacks of altering PrP primary structures at *N*-glycan linkage sites and instead relies on immunological discrimination of PrP isoforms based on covalent and conformational differences between PrP^C and PrP^{Sc}. We show that the discontinuous, conformation-dependent epitope of mAb PRC7 is occluded following glycan attachment to PrP at Asn-196. Accordingly, under uninfected conditions PRC7 only recognizes either nonglycosylated PrP, including bacterially-expressed recombinant or enzymatically deglycosylated PrP^C, or mono 1 PrP^C, but fails to recognize fully glycosylated PrP^C or mono 2 PrP^C. Our findings showing that PrP^C is comparatively refractory to PRC7 detection support the notion that this isoform is predisposed to complete glycosylation at both *N*-linkage sites. In contrast, because PRC7-reactive PrP is preferentially produced under conditions of prion infection, we conclude that hypoglycosylation is a feature of PrP^{Sc}. The consistently overlapping properties of PRC7-reactive hypoglycosylated PrP^{Sc} with conventional measures of pathogenic PrP^{Sc}, including differential resistance to protease treatment, insolubility in nondenaturing detergents, cellular proteolytic processing, kinetics of formation, and infectivity provide additional support for this conclusion.

Our findings illustrate an alternative strategy for prion detection based on the extent to which epitopes are shielded or unshielded from recognition as a result of PrP glycosylation. Targeted detection of PrP^{Sc} using mAb PRC7 precludes the requirement of biochemically distinguishing PrP^{Sc} from PrP^C

by means of their variable resistances to protease treatment, differential solubility in nondenaturing detergents, or other methods. We show that our approach facilitates prion detection in naturally occurring prion disorders, and we propose that development of reagents and processes that focus on enhanced detection of hypoglycosylated PrP^{Sc} will lead to significant improvements in prion diagnosis.

An additional notable aspect of our studies involves the correlation between emerging prion titers following infection of mice with RML prions, and the kinetics of PrP^{Sc} production as monitored not only by PRC7-reactive hypoglycosylated but also protease-resistant PrP^{Sc}, which appear to be at odds with the interpretation that replicative and toxic PrP forms are independent (55).

Specificity of PRC7 for PrP^{Sc} derives from two features of its epitope. First, whereas diminished *N*-glycan occupancy at Asn-196 in hypoglycosylated PrP^{Sc} results in epitope exposure and the potential for PRC7 recognition, optimal *N*-glycan occupancy at Asn-196 in hyperglycosylated PrP^C occludes the underlying epitope that prohibits its recognition by PRC7. This proposal is consistent with previous work suggesting that the large size and dynamic properties of the *N*-linked sugars enables them to almost completely shield two orthogonal faces of PrP (56). Second, because nonglycosylated rPrP is readily detected in the 7-5 ELISA either with or without pretreatment with GdnHCl (Fig. 5A), whereas detection of hypoglycosylated PrP^{Sc} requires GdnHCl pretreatment, we conclude that the PRC7 epitope is refractory to detection in the PrP^{Sc} conformation, and requires renaturation to its functional configuration as it occurs in the globular, largely α -helical structure of PrP^C. This interpretation is consistent with the organized location of the proposed constituent amino acid residues of the PRC7 epitope in the context of α -helical PrP^C (6) compared with their separation in the putative four-rung β -solenoid model structure of PrP^{Sc} (7) (Fig. 1, I and J). We also show that the conformational features of the unshielded PRC7 epitope in PrP^{Sc} afforded a direct and sensitive approach, referred to as 7-5 CSA, to distinguish the properties of prion strains without resorting to differential resistance to protease treatment.

Our findings also build on previously published observations. Although seminal mass spectrometric studies failed to reveal post-translational differences between PrP^C and PrP^{Sc} (57), subsequent comparisons revealed variances in the oligosaccharide pools released from PrP^C and protease-resistant PrP^{Sc} (58), a finding that is in accordance with differential glycosylation of the two isoforms. Also, in accordance with our findings using PRC5 (Fig. 2B), previous studies using similarly nondiscriminatory antibodies indicated that hypoglycosylated PrP accumulated during murine prion infection (20, 59), although the exact relationship of these observations to prion disease pathogenesis remained unclear at that time. Although mAbs recognizing glycan-controlled epitopes similar to PRC7 have been described in previous studies (21–23), their epitope specificities and capacities to preferentially recognize PrP in the infected state were not systematically investigated. Our results using PRC7 also shed light on previous reports of PrP^{Sc} detection using a mAb referred to as ICSM 10 (60). Although the mechanism by which this mAb detected PrP^{Sc} was not addressed in this study, prion

Targeting underglycosylated PrP^{Sc} as a basis for prion detection

work describing its isolation and partial characterization indicated that ICSM 10 recognizes nonglycosylated and monoglycosylated, but not fully glycosylated PrP (22). These investigators were unable to map the epitope of ICSM 10 using linear peptides in an ELISA format (22), a finding that is consistent with our findings that demonstrated that the failure of this mapping strategy results from mAbs recognizing discontinuous, conformational epitopes in the globular α -helical domain of PrP^C (24). Because PrP^{Sc} recognition by ICSM 10 required denaturation (60) we propose that, like PRC7, this reflects obligatory refolding of the ICSM 10 epitope from its unrecognized configuration in PrP^{Sc} to a functional α -helical conformation. Despite their inability to map the ICSM 10 epitope, the authors speculated that it likely spans the areas around the known sites of *N*-linked glycosylation of PrP (22). We concur and further propose that like PRC7, ICSM 10 recognizes hypoglycosylated PrP^{Sc} as a result of interaction with a conformation-dependent epitope that is occluded following glycan attachment to one of the two *N*-linkage sites of PrP. We contend that this explanation corroborates our findings with PRC7 that prions contain hypoglycosylated PrP^{Sc}. Although not addressed in previous studies (22, 60), it will be of considerable interest to discover whether the partially glycosylated PrP^{Sc} species recognized by ICSM 10 is mono 2 or, as in the case of PRC7, mono 1.

Experimental procedures

Sources of prion-infected materials

CWD prions were derived from the brains of naturally affected deer or elk, and from the brains of experimentally challenged Gt or Tg mice expressing deer or elk PrP (31, 32). Stetsonville TME prions were prepared from mink as described (61). Mouse-adapted scrapie prions, 22L, RML and 139A were isolated from the brains of WT FVB or C57Bl/6 mice. Experimentally infected animals were inoculated and monitored for development of prion disease as previously described (62).

Cell culture and monoclonal antibodies

Rabbit kidney epithelial (RK13) cells were obtained from the American Type Culture Collection (catalog number CCL-37; ATCC). PrP coding sequences containing various mutations were generated by gene synthesis (GenScript, Piscataway, NJ). Expression cassettes were engineered into the pIRESpuro3 expression vector (Takara-Clontech, Mountain View, CA), and RK13 cells were transfected with expression constructs using Lipofectamine as previously described (24). Transfected RK13 cells stably expressing PrP were selected in Dulbecco's modified Eagle's medium with 10% fetal bovine serum containing penicillin and streptomycin and 1 μ g/ml of puromycin (Sigma-Aldrich) in a regulated atmosphere containing 5% CO₂ at 37 °C. RK13 cells expressing empty pIRESpuro3 vector were used as negative controls for cell-based expression assays. Hybridoma production and purification of mAbs PRC5 and PRC7 have been described previously (24).

Prion titration

RK13 cells previously engineered to stably express mouse PrP that were highly sensitive to mouse prion infection, referred to as RK-M, were isolated by single cell dilution cloning (29). Titers of prions in the brains of FVB mice challenged with RML prions collected at various intervals post-infection were assessed in RK-M cells using a modified scrapie cell assay (28) as previously described (29, 30).

Immunoblotting methods to detect PrP

Protein concentrations in cell lysates and 10% brain homogenates were determined by bicinchoninic acid assay (Pierce Biotechnology, Rockford, IL). Equivalent amounts of total proteins were loaded on gels for comparison by Western blotting analysis. Cell culture lysates and brain homogenates were treated with PK and or PNGase F and analyzed by Western blotting as previously described (19). Membranes exposed to HRP-conjugated secondary antibody were developed using ECL 2 Western blotting substrate (Thermo Scientific, Waltham, MA) and scanned with FLA-5000 scanner (Fujifilm Life Science, Woodbridge, CT). PK-resistant PrP^{Sc} was analyzed by a dot-blot assay as previously described (12). Membranes were imaged and quantified with ImageQuant LAS 4000 and ImageQuant TL software (GE Healthcare). Analysis of PrP in coronal sections of mouse brains by histoblotting was performed according to previously described protocols (63). Images were captured with a Nikon STM DMX 1200F digital camera and analyzed using Micropublisher 6 and Ocualar imaging software (Teledyne Qimaging, Surrey, BC, Canada). To separate soluble- and insoluble-PrP, Sarkosyl was added to final 2% (w/v) to 10% brain homogenates prepared in PBS containing 50 μ g of total protein for 30 min on ice. Samples were centrifuged at 100,000 \times *g* for 1 h at 4 °C in a Beckman Coulter Optima Max-XP ultracentrifuge (Brea, CA). The resulting pellets were suspended in SDS-PAGE sample loading buffer, and supernatants were transferred to fresh tubes containing a 3 \times volume of ice-cold methanol and stored overnight at –20 °C. Proteins were isolated by centrifugation at 14,000 rpm for 10 min at 4 °C and pellets were allowed to air dry and suspended in SDS-PAGE sample loading buffer. Soluble- and insoluble-fractions thus isolated were subjected to SDS-PAGE followed by Western immunoblotting with mAbs PRC5 or PRC7 and subsequent chemiluminescent detection as described (19).

Production of recombinant PrP and analysis by indirect and sandwich ELISA

Recombinant mouse and elk PrP was produced using previously described methods (24). For indirect ELISAs, Nunc Maxi-Sorp flat-bottom 96-well– plates were coated overnight with 1 μ g of rPrP per well in carbonate-bicarbonate buffer at 4 °C. The contents of wells were either treated or not with GdnHCl to a final concentration of 5 M for 15 min at 37 °C with mixing on an orbital heat block shaker. Wells were then washed three times with 200 μ l of TBST per well. Wells were then blocked using 200 μ l of 3% BSA in PBS for 1 h at 37 °C. Wells were washed and then incubated overnight at 4 °C in either 0.2 μ g/ml of PRC5 or 0.42 μ g/ml of PRC7 prepared in 1% BSA/PBS. Wells were

washed as described previously, then incubated in HRP-conjugated secondary antibodies against mouse IgG1 (PRC7) or IgG2a (PRC5) (Alpha Diagnostics, San Antonio, TX), diluted 1:5000 in 1% BSA/PBS. For analysis of rPrP by 7-5 sandwich ELISA 96-well-plates were coated overnight with 1 µg of mAb PRC7 per well in carbonate-bicarbonate buffer at 4 °C. Separately, rPrP was treated with 1% Triton X-100 in PBS for 1 h at 37 °C with mixing. Samples were either treated or not with GdnHCl to a final concentration of 5 M for 15 min at 37 °C with mixing. Sample volumes were then diluted to a final GdnHCl concentration of 0.5 M using 1% BSA/PBS. Plates were blocked with 200 µl of 3% BSA in PBS/well for 1 h at 37 °C and washed three times with TBST. Treated rPrP was captured by PRC7 overnight at 4 °C and then washed three times with 200 µl of TBST/well. PRC5 in 1% BSA/PBS was added (0.2 µg/ml) for 1 h at 37 °C followed by washes and then HRP-conjugated secondary antibody against mouse IgG2a (Alpha Diagnostics). Wells were washed and then developed using tetramethylbenzidine for 30 s and reactions were stopped by addition of 2 M H₂SO₄. Absorbance was read at 450 nm using a Bio-Tek Elx808 Ultra Microplate Reader (Bio-Tek instruments, Inc., Winooski, VT).

Sandwich ELISA modifications for assays of brain extracts

For the analyzes of brain extracts by 13-5 and 7-5 ELISA, 96-well-plates were coated with 2 µg of mAb D13 or 1 µg of mAb PRC7 as described above. Prior to capture with mAb D13 or mAb PRC7, brain homogenates were solubilized in 1% Triton X-100/PBS. For denaturation, samples were treated with a final concentration of 5 M GdnHCl as described above. Samples were serially diluted to achieve capture of 20, 10, 5, 2.5, 1.25, or 0.625 µg of protein per well performed in technical triplicates. Experiments involving natural isolates captured 20 µg/well. Plates were processed as described above and developed using 2,2'-azino-di(3-ethylbenzathiazoline-6-sulfonate) (ABTS) substrate (1-Component) (Seracare Life Sciences, Milford, MA) at room temperature, and reactions were stopped with ABTS Stop Solution (Seracare Life Sciences, Milford, MA) after 15 to 20 min. Absorbance was read at 405 nm using a Bio-Tek Elx808 Ultra Microplate Reader (Bio-Tek instruments, Inc.).

7-5 CSA

Brain extracts containing 20 µg of total protein per well were subjected to half-molar gradient increases of GdnHCl between 0 and 5 M and incubated at 37 °C for 15 min with mixing, followed by the 7-5 ELISA protocol outlined above. Samples were treated with or without 50 µg/ml of PK for 1 h at 37 °C and mixing. Digestion was terminated by adding PMSF to a final concentration of 2 mM.

Molecular modeling and statistical analysis

Molecular models of PrP^C were generated using iMol for Mac OS X (RRID:SCR_018735). All statistical analysis were performed using GraphPad Prism software (San Diego, CA).

Animal care and use

Animal work was performed in compliance with the requirements of University Institutional Animal Care and Use Committees.

Acknowledgments—We thank Dr. Carol Wilusz for helpful perspectives and editorial suggestions. We acknowledge the technical assistance of Carla Calvi, Toru Ishii, and Deandra Walker during developmental aspects of this work. We thank Prionics for supplying mAb 6H4. We thank our various collaborators for supplying materials from CWD-affected deer and elk.

Author contributions—H-E. K. and G. C. T. conceptualization; H-E. K., J. B., S. J. K., S. K., V. S., and J. C. data curation; H-E. K., J. B., S. J. K., and G. C. T. formal analysis; H-E. K. and G. C. T. supervision; H-E. K., J. B., S. J. K., and J. C. validation; H-E. K., J. B., S. J. K., V. S., J. C., and G. C. T. investigation; H-E. K., J. B., S. J. K., S. K., V. S., J. C., and G. C. T. methodology; S. J. K., J. C. B., and G. C. T. writing-review and editing; J. C. B. and G. C. T. resources; G. C. T. funding acquisition; G. C. T. visualization; G. C. T. writing-original draft; G. C. T. project administration.

Funding and additional information—This work was supported by National Institutes of Health Grants RO1NS040334, RO1NS109376, RO1NS103763, and PO0011877A. The content is solely the responsibility of the authors and does not represent the official views of the National Institutes of Health.

Conflict of interest—The authors declare that they have no conflicts of interest with the contents of this article.

Abbreviations—The abbreviations used are: CWD, chronic wasting disease; rPrP, recombinant PrP; PNGase F, peptide:N-glycosidase F; PK, proteinase K; MoPrP, mouse PrP; rPrP, recombinant PrP; TME, transmissible mink encephalopathy; Tg, transgenic; 7-5 CSA, 7-5 conformational stability analysis; GdnHCl guanidine hydrochloride.

References

- Will, R. G., Ironside, J. W., Zeidler, M., Cousens, S. N., Estibeiro, K., Alperovitch, A., Poser, S., Pocchiari, M., Hofman, A., and Smith, P. G. (1996) A new variant of Creutzfeldt-Jakob disease in the UK. *Lancet* **347**, 921–925 [CrossRef Medline](#)
- Benestad, S. L., and Telling, G. C. (2018) Chronic wasting disease: an evolving prion disease of cervids. *Handb. Clin. Neurol.* **153**, 135–151 [CrossRef Medline](#)
- Babelhadj, B., Di Bari, M. A., Pirisinu, L., Chiappini, B., Gaouar, S. B. S., Riccardi, G., Marcon, S., Agrimi, U., Nonno, R., and Vaccari, G. (2018) Prion disease in Dromedary camels, Algeria. *Emerg. Infect. Dis.* **24**, 1029–1036 [CrossRef Medline](#)
- Prusiner, S. B. (1982) Novel proteinaceous infectious particles cause scrapie. *Science* **216**, 136–144 [CrossRef Medline](#)
- Prusiner, S. B. (1998) Prions (Les Prix Nobel Lecture). in *Les Prix Nobel* (Frängsmyr, T., ed) pp. 268–323, Almquist & Wiksell International, Stockholm, Sweden
- Riek, R., Hornemann, S., Wider, G., Billeter, M., Glockshuber, R., and Wüthrich, K. (1996) NMR structure of the mouse prion protein domain PrP(121–231). *Nature* **382**, 180–182 [CrossRef Medline](#)
- Spagnoli, G., Rigoli, M., Orioli, S., Sevilano, A. M., Faccioli, P., Wille, H., Biasini, E., and Requena, J. R. (2019) Full atomistic model of prion structure and conversion. *PLoS Pathog.* **15**, e1007864 [CrossRef Medline](#)

8. Korth, C., Stierli, B., Streit, P., Moser, M., Schaller, O., Fischer, R., Schulz-Schaeffer, W., Kretzschmar, H., Raeber, A., Braun, U., Ehrensperger, F., Hornemann, S., Glockshuber, R., Riek, R., Billeter, M., *et al.* (1997) Prion (PrP^{Sc})-specific epitope defined by a monoclonal antibody. *Nature* **390**, 74–77 [CrossRef Medline](#)
9. Nazor, K. E., Kuhn, F., Seward, T., Green, M., Zwald, D., Pürro, M., Schmid, J., Biffiger, K., Power, A. M., Oesch, B., Raeber, A. J., and Telling, G. C. (2005) Immunodetection of disease-associated mutant PrP, which accelerates disease in GSS transgenic mice. *EMBO J.* **24**, 2472–2480 [CrossRef Medline](#)
10. Biasini, E., Seegulam, M. E., Patti, B. N., Solforosi, L., Medrano, A. Z., Christensen, H. M., Senatore, A., Chiesa, R., Williamson, R. A., and Harris, D. A. (2008) Non-infectious aggregates of the prion protein react with several PrP(Sc)-directed antibodies. *J. Neurochem.* **105**, 2190–2204 [CrossRef Medline](#)
11. Li, J., Browning, S., Mahal, S. P., Oelschlegel, A. M., and Weissmann, C. (2010) Darwinian evolution of prions in cell culture. *Science* **327**, 869–872 [CrossRef Medline](#)
12. Bian, J., Kang, H. E., and Telling, G. (2014) Quinacrine promotes replication and conformational mutation of chronic wasting disease prions. *Proc. Natl. Acad. Sci. U.S.A.* **111**, 6028–6033 [CrossRef](#)
13. Bruce, M., Chree, A., McConnell, I., Foster, J., Pearson, G., and Fraser, H. (1994) Transmission of bovine spongiform encephalopathy and scrapie to mice: strain variation and the species barrier. *Phil. Trans. R. Soc. Lond. B* **343**, 405–411 [CrossRef](#)
14. Bessen, R. A., and Marsh, R. F. (1994) Distinct PrP properties suggest the molecular basis of strain variation in transmissible mink encephalopathy. *J. Virol.* **68**, 7859–7868 [CrossRef Medline](#)
15. Telling, G. C., Parchi, P., DeArmond, S. J., Cortelli, P., Montagna, P., Gabizon, R., Mastrianni, J., Lugaresi, E., Gambetti, P., and Prusiner, S. B. (1996) Evidence for the conformation of the pathologic isoform of the prion protein enciphering and propagating prion diversity. *Science* **274**, 2079–2082 [CrossRef Medline](#)
16. Pan, K. M., Stahl, N., and Prusiner, S. B. (1992) Purification and properties of the cellular prion protein from Syrian hamster brain. *Protein Sci.* **1**, 1343–1352 [CrossRef Medline](#)
17. Harris, D. A., Huber, M. T., van Dijken, P., Shyng, S.-L., Chait, B. T., and Wang, R. (1993) Processing of a cellular prion protein: identification of N- and C-terminal cleavage sites. *Biochemistry* **32**, 1009–1016 [CrossRef Medline](#)
18. Chen, S. G., Teplow, D. B., Parchi, P., Teller, J. K., Gambetti, P., and Autioli-Gambetti, L. (1995) Truncated forms of the human prion protein in normal brain and in prion diseases. *J. Biol. Chem.* **270**, 19173–19180 [CrossRef Medline](#)
19. Yadavalli, R., Guttman, R. P., Seward, T., Centers, A. P., Williamson, R. A., and Telling, G. C. (2004) Calpain-dependent endoproteolytic cleavage of PrP^{Sc} modulates scrapie prion propagation. *J. Biol. Chem.* **279**, 21948–21956 [CrossRef Medline](#)
20. Pan, T., Li, R., Wong, B. S., Liu, T., Gambetti, P., and Sy, M. S. (2002) Heterogeneity of normal prion protein in two-dimensional immunoblot: presence of various glycosylated and truncated forms. *J. Neurochem.* **81**, 1092–1101 [CrossRef Medline](#)
21. Polymenidou, M., Moos, R., Scott, M., Sigurdson, C., Shi, Y. Z., Yajima, B., Hafner-Bratkovic, I., Jerala, R., Hornemann, S., Wuthrich, K., Bellon, A., Vey, M., Garen, G., James, M. N., Kav, N., *et al.* (2008) The POM monoclonals: a comprehensive set of antibodies to non-overlapping prion protein epitopes. *PLoS ONE* **3**, e3872 [CrossRef Medline](#)
22. Khalili-Shirazi, A., Summers, L., Linehan, J., Mallinson, G., Anstee, D., Hawke, S., Jackson, G. S., and Collinge, J. (2005) PrP glycoforms are associated in a strain-specific ratio in native PrP^{Sc}. *J. Gen. Virol.* **86**, 2635–2644 [CrossRef Medline](#)
23. Moudjou, M., Treguer, E., Rezaei, H., Sabuncu, E., Neuendorf, E., Groschup, M. H., Grosclaude, J., Laude, H., and Neuendorf, E. (2004) Glycan-controlled epitopes of prion protein include a major determinant of susceptibility to sheep scrapie. *J. Virol.* **78**, 9270–9276 [CrossRef Medline](#)
24. Kang, H. E., Weng, C. C., Saijo, E., Saylor, V., Bian, J., Kim, S., Ramos, L., Angers, R., Langenfeld, K., Khaychuk, V., Calvi, C., Bartz, J., Hunter, N., and Telling, G. C. (2012) Characterization of conformation-dependent prion protein epitopes. *J. Biol. Chem.* **287**, 37219–37232 [CrossRef Medline](#)
25. Mays, C. E., Kim, C., Haldiman, T., van der Merwe, J., Lau, A., Yang, J., Grams, J., Di Bari, M. A., Nonno, R., Telling, G. C., Kong, Q., Langeveld, J., McKenzie, D., Westaway, D., and Safar, J. G. (2014) Prion disease tempo determined by host-dependent substrate reduction. *J. Clin. Invest.* **124**, 847–858 [CrossRef Medline](#)
26. Matsunaga, Y., Peretz, D., Williamson, A., Burton, D., Mehlhorn, I., Groth, D., Cohen, F. E., Prusiner, S. B., and Baldwin, M. A. (2001) Cryptic epitopes in N-terminally truncated prion protein are exposed in the full-length molecule: dependence of conformation on pH. *Proteins* **44**, 110–118 [CrossRef Medline](#)
27. Safar, J., Wille, H., Itri, V., Groth, D., Serban, H., Torchia, M., Cohen, F. E., and Prusiner, S. B. (1998) Eight prion strains have PrP^{Sc} molecules with different conformations. *Nat. Med.* **4**, 1157–1165 [CrossRef Medline](#)
28. Klöhn, P. C., Stoltze, L., Flechsig, E., Enari, M., and Weissmann, C. (2003) A quantitative, highly sensitive cell-based infectivity assay for mouse scrapie prions. *Proc. Natl. Acad. Sci. U.S.A.* **100**, 11666–11671 [CrossRef Medline](#)
29. Bian, J., Khaychuk, V., Angers, R. C., Fernández-Borges, N., Vidal, E., Meyerett-Reid, C., Kim, S., Calvi, C. L., Bartz, J. C., Hoover, E. A., Agrimi, U., Richt, J. A., Castilla, J., and Telling, G. C. (2017) Prion replication without host adaptation during interspecies transmissions. *Proc. Natl. Acad. Sci. U.S.A.* **114**, 1141–1146 [CrossRef Medline](#)
30. Bian, J., Napier, D., Khaychuk, V., Angers, R., Graham, C., and Telling, G. (2010) Cell-based quantification of chronic wasting disease prions. *J. Virol.* **84**, 8322–8326 [CrossRef Medline](#)
31. Bian, J., Christiansen, J. R., Moreno, J. A., Kane, S. J., Khaychuk, V., Gallegos, J., Kim, S., and Telling, G. C. (2019) Primary structural differences at residue 226 of deer and elk PrP dictate selection of distinct CWD prion strains in gene-targeted mice. *Proc. Natl. Acad. Sci. U.S.A.* **116**, 12478–12487 [CrossRef Medline](#)
32. Angers, R. C., Kang, H. E., Napier, D., Browning, S., Seward, T., Mathiason, C., Balachandran, A., McKenzie, D., Castilla, J., Soto, C., Jewell, J., Graham, C., Hoover, E. A., and Telling, G. C. (2010) Prion strain mutation determined by prion protein conformational compatibility and primary structure. *Science* **328**, 1154–1158 [CrossRef Medline](#)
33. Peretz, D., Scott, M. R., Groth, D., Williamson, R. A., Burton, D. R., Cohen, F. E., and Prusiner, S. B. (2001) Strain-specified relative conformational stability of the scrapie prion protein. *Protein Sci.* **10**, 854–863 [CrossRef Medline](#)
34. Mitra, N., Sinha, S., Ramya, T. N., and Surolia, A. (2006) N-Linked oligosaccharides as outfitters for glycoprotein folding, form and function. *Trends Biochem. Sci.* **31**, 156–163 [CrossRef Medline](#)
35. Hanson, S. R., Culyba, E. K., Hsu, T. L., Wong, C. H., Kelly, J. W., and Powers, E. T. (2009) The core trisaccharide of an N-linked glycoprotein intrinsically accelerates folding and enhances stability. *Proc. Natl. Acad. Sci. U.S.A.* **106**, 3131–3136 [CrossRef Medline](#)
36. Cancellotti, E., Barron, R. M., Bishop, M. T., Hart, P., Wiseman, F., and Manson, J. C. (2007) The role of host PrP in transmissible spongiform encephalopathies. *Biochim. Biophys. Acta* **1772**, 673–680 [CrossRef Medline](#)
37. Wiseman, F. K., Cancellotti, E., Piccardo, P., Iremonger, K., Boyle, A., Brown, D., Ironside, J. W., Manson, J. C., and Diack, A. B. (2015) The glycosylation status of PrP^C is a key factor in determining transmissible spongiform encephalopathy transmission between species. *J. Virol.* **89**, 4738–4747 [CrossRef Medline](#)
38. Neuendorf, E., Weber, A., Saalmueller, A., Schatzl, H., Reifenberg, K., Pfaff, E., and Groschup, M. H. (2004) Glycosylation deficiency at either one of the two glycan attachment sites of cellular prion protein preserves susceptibility to bovine spongiform encephalopathy and scrapie infections. *J. Biol. Chem.* **279**, 53306–53316 [CrossRef Medline](#)
39. Piro, J. R., Harris, B. T., Nishina, K., Soto, C., Morales, R., Rees, J. R., and Supattapone, S. (2009) Prion protein glycosylation is not required for strain-specific neurotropism. *J. Virol.* **83**, 5321–5328 [CrossRef Medline](#)
40. Katorcha, E., Makarava, N., Savtchenko, R., D'Azzo, A., and Baskakov, I. V. (2014) Sialylation of prion protein controls the rate of prion amplification,

- the cross-species barrier, the ratio of PrP^{Sc} glycoform and prion infectivity. *PLoS Pathog.* **10**, e1004366 [CrossRef Medline](#)
41. Moudjou, M., Chapuis, J., Mekrouti, M., Reine, F., Herzog, L., Sibille, P., Laude, H., Vilette, D., Andréoletti, O., Rezaei, H., Dron, M., and Béringue, V. (2016) Glycoform-independent prion conversion by highly efficient, cell-based, protein misfolding cyclic amplification. *Sci. Rep.* **6**, 29116 [CrossRef Medline](#)
42. Nishina, K. A., Deleault, N. R., Mahal, S. P., Baskakov, I., Luhrs, T., Riek, R., and Supattapone, S. (2006) The stoichiometry of host PrP^C glycoforms modulates the efficiency of PrP^{Sc} formation *in vitro*. *Biochemistry* **45**, 14129–14139 [CrossRef Medline](#)
43. Camacho, M. V., Telling, G., Kong, Q., Gambetti, P., and Notari, S. (2019) Role of prion protein glycosylation in replication of human prions by protein misfolding cyclic amplification. *Lab. Invest.* **99**, 1741–1748 [CrossRef Medline](#)
44. Rogers, M., Taraboulos, A., Scott, M., Groth, D., and Prusiner, S. B. (1990) Intracellular accumulation of the cellular prion protein after mutagenesis of its Asn-linked glycosylation sites. *Glycobiology* **1**, 101–109 [CrossRef Medline](#)
45. DeArmond, S. J., Sanchez, H., Yehiely, F., Qiu, Y., Ninchak-Casey, A., Daggett, V., Camerino, A. P., Cayetano, J., Rogers, M., Groth, D., Torchia, M., Tremblay, P., Scott, M. R., Cohen, F. E., and Prusiner, S. B. (1997) Selective neuronal targeting in prion disease. *Neuron* **19**, 1337–1348 [CrossRef Medline](#)
46. Cancellotti, E., Wiseman, F., Tuzi, N. L., Baybutt, H., Monaghan, P., Aitchison, L., Simpson, J., and Manson, J. C. (2005) Altered glycosylated PrP proteins can have different neuronal trafficking in brain but do not acquire scrapie-like properties. *J. Biol. Chem.* **280**, 42909–42918 [CrossRef Medline](#)
47. Tuzi, N. L., Cancellotti, E., Baybutt, H., Blackford, L., Bradford, B., Plinston, C., Coghill, A., Hart, P., Piccardo, P., Barron, R. M., and Manson, J. C. (2008) Host PrP glycosylation: a major factor determining the outcome of prion infection. *PLoS Biol.* **6**, e100 [CrossRef Medline](#)
48. Cancellotti, E., Bradford, B. M., Tuzi, N. L., Hickey, R. D., Brown, D., Brown, K. L., Barron, R. M., Kisielewski, D., Piccardo, P., and Manson, J. C. (2010) Glycosylation of PrP^C determines timing of neuroinvasion and targeting in the brain following transmissible spongiform encephalopathy infection by a peripheral route. *J. Virol.* **84**, 3464–3475 [CrossRef Medline](#)
49. Korth, C., Kaneko, K., and Prusiner, S. B. (2000) Expression of unglycosylated mutated prion protein facilitates PrP(Sc) formation in neuroblastoma cells infected with different prion strains. *J. Gen. Virol.* **81**, 2555–2563 [CrossRef Medline](#)
50. Capellari, S., Zaidi, S. I., Long, A. C., Kwon, E. E., and Petersen, R. B. (2000) The Thr183-Ala mutation, not the loss of the first glycosylation site, alters the physical properties of the prion protein. *J. Alzheimers Dis.* **2**, 27–35 [CrossRef Medline](#)
51. Asante, E. A., Smidak, M., Grimshaw, A., Houghton, R., Tomlinson, A., Jeelani, A., Jakubcova, T., Hamdan, S., Richard-Londt, A., Linehan, J. M., Brandner, S., Alpers, M., Whitfield, J., Mead, S., Wadsworth, J. D., et al. (2015) A naturally occurring variant of the human prion protein completely prevents prion disease. *Nature* **522**, 478–481 [CrossRef Medline](#)
52. Wadsworth, J. D., Asante, E. A., Desbruslais, M., Linehan, J. M., Joiner, S., Gowland, I., Welch, J., Stone, L., Lloyd, S. E., Hill, A. F., Brandner, S., and Collinge, J. (2004) Human prion protein with valine 129 prevents expression of variant CJD phenotype. *Science* **306**, 1793–1796 [CrossRef Medline](#)
53. Green, K. M., Browning, S. R., Seward, T. S., Jewell, J. E., Ross, D. L., Green, M. A., Williams, E. S., Hoover, E. A., and Telling, G. C. (2008) The elk PRNP codon 132 polymorphism controls cervid and scrapie prion propagation. *J. Gen. Virol.* **89**, 598–608 [CrossRef Medline](#)
54. Angers, R., Christiansen, J., Nalls, A. V., Kang, H. E., Hunter, N., Hoover, E., Mathiason, C. K., Sheetz, M., and Telling, G. C. (2014) Structural effects of PrP polymorphisms on intra- and interspecies prion transmission. *Proc. Natl. Acad. Sci. U.S.A.* **111**, 11169–11174 [CrossRef Medline](#)
55. Sandberg, M. K., Al-Doujaily, H., Sharps, B., Clarke, A. R., and Collinge, J. (2011) Prion propagation and toxicity *in vivo* occur in two distinct mechanistic phases. *Nature* **470**, 540–542 [CrossRef Medline](#)
56. Rudd, P. M., Wormald, M. R., Wing, D. R., Prusiner, S. B., and Dwek, R. A. (2001) Prion glycoprotein: structure, dynamics, and roles for the sugars. *Biochemistry* **40**, 3759–3766 [CrossRef Medline](#)
57. Stahl, N., Baldwin, M. A., Teplow, D. B., Hood, L., Gibson, B. W., Burlingame, A. L., and Prusiner, S. B. (1993) Structural studies of the scrapie prion protein using mass spectrometry and amino acid sequencing. *Biochemistry* **32**, 1991–2002 [CrossRef Medline](#)
58. Rudd, P. M., Endo, T., Colominas, C., Groth, D., Wheeler, S. F., Harvey, D. J., Wormald, M. R., Serban, H., Prusiner, S. B., Kobata, A., and Dwek, R. A. (1999) Glycosylation differences between the normal and pathogenic prion protein isoforms. *Proc. Natl. Acad. Sci. U.S.A.* **96**, 13044–13049 [CrossRef Medline](#)
59. Russelakis-Carneiro, M., Saborio, G. P., Anderes, L., and Soto, C. (2002) Changes in the glycosylation pattern of prion protein in murine scrapie. Implications for the mechanism of neurodegeneration in prion diseases. *J. Biol. Chem.* **277**, 36872–36877 [CrossRef Medline](#)
60. Tattum, M. H., Jones, S., Pal, S., Khalili-Shirazi, A., Collinge, J., and Jackson, G. S. (2010) A highly sensitive immunoassay for the detection of prion-infected material in whole human blood without the use of proteinase K. *Transfusion* **50**, 2619–2627 [CrossRef Medline](#)
61. Bartz, J. C., Bessen, R. A., McKenzie, D., Marsh, R. F., and Aiken, J. M. (2000) Adaptation and selection of prion protein strain conformations following interspecies transmission of transmissible mink encephalopathy. *J. Virol.* **74**, 5542–5547 [CrossRef Medline](#)
62. Green, K. M., Castilla, J., Seward, T. S., Napier, D. L., Jewell, J. E., Soto, C., and Telling, G. C. (2008) Accelerated high fidelity prion amplification within and across prion species barriers. *PLoS Pathog.* **4**, e1000139 [CrossRef Medline](#)
63. Taraboulos, A., Jendroska, K., Serban, D., Yang, S. L., DeArmond, S. J., and Prusiner, S. B. (1992) Regional mapping of prion proteins in brain. *Proc. Natl. Acad. Sci. U.S.A.* **89**, 7620–7624 [CrossRef Medline](#)